

Contents lists available at ScienceDirect

Quaternary Science Reviews

journal homepage: www.elsevier.com/locate/quascirev



The dynamics of warming during the last deglaciation in highelevation regions of Eastern Equatorial Africa



Sloane Garelick ^{a, *}, James Russell ^a, Adin Richards ^a, Jamila Smith ^{a, b}, Meredith Kelly ^c, Nathan Anderson ^c, Margaret S. Jackson ^{c, d}, Alice Doughty ^e, Bob Nakileza ^f, Sarah Ivory ^{g, h}, Sylvia Dee ⁱ, Charlie Marshall ⁱ

- ^a Dept. of Earth, Environmental and Planetary Sciences, Brown University, Providence, RI, USA
- ^b State University of New York at Fredonia, Fredonia, NY, USA
- ^c Dept. of Earth Science, Dartmouth College, Hanover, NH, USA
- ^d Geography, School of Natural Sciences, Trinity College Dublin, Dublin, Ireland
- e School of Earth and Climate Sciences, University of Maine, Orono, ME, USA
- f Makerere University, Mountain Resource Centre, Kampala, Uganda
- g Dept. of Geosciences, Pennsylvania State University, State College, PA, USA
- ^h Earth and Environmental Systems Institute, Pennsylvania State University, State College, PA, USA
- ⁱ Dept. of Earth, Environmental and Planetary Sciences, Rice University, Houston, TX, USA

ARTICLE INFO

Article history: Received 29 September 2021 Received in revised form 31 January 2022 Accepted 3 February 2022 Available online 23 February 2022

Handling Editor: Dr Yan Zhao

Keywords:
East africa
Tropical lapse rate
Temperature
Mountain glaciers
Last glacial maximum
Holocene
Paleoclimatology
Organic geochemistry

ABSTRACT

Tropical mountain environments, such as the Rwenzori Mountains in equatorial Africa, are thought to be particularly sensitive to climate change. Ongoing warming in the Rwenzori is impacting local environments and communities through glacial retreat, fires, and flooding. Paleoclimate reconstructions from elsewhere in Africa suggest considerable warming accompanied glacier retreat during the last glacial termination, from ~21 thousand years before present (ka) through the early to mid-Holocene. Quantifying these changes has been difficult but could help to assess future impacts in the Rwenzori. Here, we present a ~21 thousand-year (kyr) temperature reconstruction based on the relative abundance of branched glycerol dialkyl glycerol tetraethers (brGDGTs) from Lake Mahoma (2,990 m above sea level; m asl) in the Rwenzori Mountains, Uganda. Our record, paired with existing Rwenzori glacial moraine ¹⁰Be exposure ages, suggests that deglacial warming and glacial retreat began by ~20 ka and accelerated at ~18-18.5 ka. The timing of the onset of rapid warming matches the timing of the post-glacial rise in radiative forcing from atmospheric greenhouse gases (GHGs) from Antarctic ice cores (Brook et al., 1996; Marcott et al., 2014; Monnin et al., 2004; Schilt et al., 2010). Our temperature reconstruction registers ~4.9 °C warming from the Last Glacial Maximum (LGM) to the late Holocene. This increase is larger than the average ~2-4 °C warming observed in records from lower elevation sites in tropical East Africa, but similar to that observed at other high-elevation sites in this region. The increased warming at higher elevations thus confirms that the temperature lapse rate steepened during the LGM over this region. Our results also indicate ~3 °C of warming during the mid-Holocene relative to the late Holocene. This suggests that the freezing-level height rose above Rwenzori summit elevations at that time, likely causing complete deglaciation of the Rwenzori Mountains from ~5 to 7 ka. The mid-Holocene is thus a potential analog for the glacial and environmental changes that these mountains are likely to experience in the coming decades. Overall, the timing and magnitude of temperature change observed in our record has important implications for climate model projections of future warming in tropical Africa.

© 2022 Elsevier Ltd. All rights reserved.

1. Introduction

As Earth's climate continues to warm, tropical mountain environments are predicted to experience a magnitude of warming second only to the Arctic. This is due to shoaling of the tropical

^{*} Corresponding author. E-mail address: sloane_garelick@brown.edu (S. Garelick).

temperature lapse rate (Collins et al., 2013), the decrease in temperature with increasing elevation. Many tropical mountain environments are home to unique, endemic flora and fauna, highaltitude tropical glaciers, and local communities that depend on these environments for income from business, tourism, and agriculture (Niang et al., 2014). Therefore, it is important to accurately predict future temperature changes, as well as changes in the temperature lapse rate, using climate models, theory, and data, but observational records from tropical mountains generally only span the past few decades and are in some cases completely unavailable. Thus, reconstructions of tropical mountain climates provide one of the only means to determine the responses of tropical mountains to global climate forcing, and thus test and help to improve climate-model predictions.

The Last Glacial Maximum (LGM; ~25-19 ka) and subsequent deglaciation is an important target for understanding future climate changes, because it is an interval of time with high rates of temperature change and is the most recent time when global warming was accompanied by a large increase in atmospheric greenhouse-gas (GHG) concentrations (Clark et al., 2009; Shakun et al., 2012). Previous studies examining changes in highelevation temperature and the temperature lapse rate during this interval indicate a discrepancy between the tropical sea surface temperature (SST) and the degree of snowline depression during the LGM (e.g., Kageyama et al., 2005; Loomis et al., 2017; Mark et al., 2005; Porter, 2000; Tripati et al., 2014). Models and proxy reconstructions generally suggest that tropical SSTs were ~2-4 °C cooler during the LGM than today (Tierney et al., 2020; Waelbroeck et al., 2009). However, evidence from changes in tropical snowline elevations suggest that LGM to present warming in high tropical mountains may have been as large as ~5-10 °C (Kageyama et al., 2005; Porter, 2000; Webster and Streten, 1978). One explanation for the discrepancy between tropical SST and tropical snowline elevations during the LGM is a change in the temperature lapse rate (Kageyama et al., 2005; Loomis et al., 2017; Tripati et al., 2014); however, this remains contentious. Tripati et al. (2014) assessed changes in tropical lapse rate based on a proxy record of SSTs from the Indo-Pacific Warm Pool and calculations of the thermal structure of the present-day atmosphere. They found that the lapse rate in both the LGM and modern were similar, suggesting minimal change between these two time periods. In contrast, Loomis et al. (2017) used proxy-based temperature reconstructions from lake sediments at different elevations in tropical East Africa to examine LGM to present temperature changes. They found that the temperature lapse rate in tropical East Africa was -6.7 °C/km during the LGM and -5.8 °C/km today, suggesting the lapse rate steepened by 0.9 °C/km during the LGM, likely due to decreased atmospheric moisture during this time. In contrast, climate model simulations suggest relatively small changes in the temperature lapse rate and the amount of warming at high-elevation sites in tropical East Africa from the LGM to present (Kageyama et al., 2005; Loomis et al., 2017), despite evidence for large changes in tropical glacial snowlines (Mark et al., 2005). Recent temperature reconstructions based on noble gases of ancient groundwater suggested that low to midlatitude land surfaces cooled by ~5.8 °C during the LGM (Seltzer et al., 2021), suggesting that previous low-elevation temperature reconstructions from tropical Africa underestimate past temperature change. However, the noble gas reconstructions include only three sites within the tropics, whereas numerous reconstructions based on organic geochemical (e.g., Loomis et al., 2012; Powers et al., 2005; Tierney et al., 2008) and fossil pollen (e.g., Bonnefille et al., 1990) from low-elevation tropical Africa indicate 2-4 °C cooling during the LGM.

To date, temperature reconstructions derived from organic geochemical proxies applied to sediment cores collected at Lake Rutundu and Sacred Lake, located at 3,078 and 2,350 m above sea level (m asl), respectively, on Mt. Kenya, (Loomis et al., 2012, 2017), are the only existing proxy-based records from high-elevation sites in tropical East Africa that extend back to the LGM. Previous work in tropical East African mountains has evaluated the timing of climate change since the LGM via changes in glacial extent (Jackson et al., 2019, 2020; Kelly et al., 2014). Although tropical glaciers are extremely sensitive to temperature (Doughty et al., 2020), it is challenging to estimate quantitative temperatures from glacial records alone. Additional proxy-based temperature reconstructions from high-elevation tropical mountains may thus improve our knowledge of past changes in the tropical temperature lapse rate and clarify existing uncertainties.

Here, we present a new ~21-kyr temperature record from the high-elevation Lake Mahoma (2,990 m asl) in the Rwenzori Mountains (Uganda). Our record is based on branched glyercol dialkyl glycerol tetraethers (brGDGTs), membrane lipids produced by bacteria and preserved in lake sediments that are increasingly being used as a temperature proxy (Weijers et al., 2007). We compare the Lake Mahoma temperature reconstruction to existing records of glacial retreat and palynological reconstructions from the Rwenzori Mountains to improve the understanding of past climate changes and their environmental impacts. Additionally, we compare the Lake Mahoma temperature record to existing LGM to present temperature records from tropical East Africa and assess regional changes in temperature and the tropical temperature lapse rate.

2. Study site

Lake Mahoma is located in the Rwenzori Mountains (0.3452°N, 29.96813°E), located on the border between Uganda and the Democratic Republic of Congo in equatorial East Africa (Fig. 1A and 1B). The Rwenzori Mountains have experienced several periods of glaciation that formed deep glacially carved valleys including the Bujuku, Mubuku, Nyamugasani, and Moulyambouli Valleys, which contain large, well-preserved moraines in the valley mouths and on the valley floors (Osmaston, 1965). Rwenzori glaciers have significantly retreated over the past century (Russell et al., 2009; Taylor et al., 2006) and today are only present above ~4,800 m asl (Kaser and Osmaston, 2002; Kelly et al., 2014). However, during the LGM, glacial moraines in the Mubuku Valley indicate that Rwenzori glaciers extended to ~2,070 m asl (Kelly et al., 2014).

Lake Mahoma is a moraine-dammed lake situated within the right lateral LGM moraines near the convergence of the Mubuku and Bujuku Valleys (Kelly et al., 2014). The lake likely filled with water and sedimentation began upon deglaciation from the moraines at ~21 ka (Jackson et al., 2019). Today, Lake Mahoma is a freshwater, acidic, oligotrophic lake with a surface area of ~4.7 ha and a maximum depth of ~25 m (Eggermont et al., 2007). Modernday vegetation in the Rwenzori is characterized by four primary vegetation zones: the montane rainforest zone (~1,800-2,400 m asl), the bamboo zone (~2,300-3,000 m asl), the ericaceous belt (~2,700-3,900 m asl), and the alpine belt (>3,800 m asl; Livingstone, 1967). Currently, Lake Mahoma is located on the boundary between the bamboo and ericaceous zones. The modern mean annual air temperature (MAAT) at the elevation of Lake Mahoma (2,990 m asl) is ~10 °C (Loomis et al., 2017). Although there is significant diurnal temperature change, there is minimal seasonal variation in temperature in the Rwenzori given the equatorial location (Livingstone, 1967). The Rwenzori Mountains experience two rainy seasons from October to November and March to May, reflecting the two-time per year passage of the Tropical Rain Belt through the area (Osmaston, 1965). Annual rainfall in the Rwenzori averages 2,500 mm/yr, with monthly

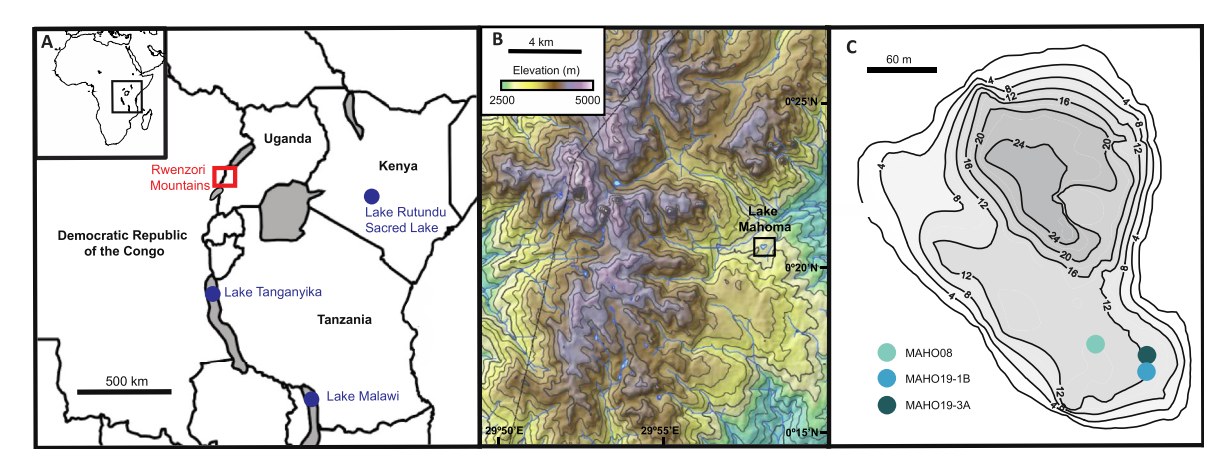


Fig. 1. A) Map of equatorial East Africa with locations of existing LGM to present GDGT-based temperature records shown with blue circles and the location of the Rwenzori Mountains shown with a red rectangle. B) Topographic map of the Rwenzori Mountains (modified from Kelly et al., 2014) with elevation contours in 200-m intervals. Lake Mahoma (black rectangle) is located in the Mubuku Valley. C) Bathymetric map of Lake Mahoma showing the locations of the three cores used to create the composite core. Contours are in 4-m intervals and represent water depth. (For interpretation of the references to colour in this figure legend, the reader is referred to the Web version of this article.)

rainfall amounts ranging from 80 to 100 mm/month during the dry seasons and as much as 400 mm/month during the wet seasons (Russell et al., 2009).

3. Methods

3.1. Core collection, imaging and dating

Sediment cores were recovered from Lake Mahoma in January 2008 (MAHO08) and January 2019 (MAHO19) (Fig. 1C). MAHO08 (0.3449°N, 29.96801°E) consisted of four cores recovered from a single hole (2P–I, 2P-II, 2P-III, 2P-IV) from a water depth of 13.2 m. The first core of MAHO08 was collected using a Bolivia corer in a polycarbonate tube and the remaining three cores were collected using a Livingstone square-rod piston corer and extruded on site. The MAHO19 sites included two adjacent holes (MAHO19-3A and MAHO19-1B) taken at offset depths in 1-m intervals using a Livingstone square-rod piston corer. MAHO19-3A (0.3452°N, 29.96813°E) consisted of four cores (1P, 2P, 3P, 4P) collected from a water depth of 11.5 m, and MAHO19-1B (0.34513°N, 29.96817°E) consisted of three cores (1P, 2P, 3P) and was collected from a water depth of 11.8 m.

We split the cores lengthwise, and then imaged and scanned the cores for magnetic susceptibility on a GeoTek multi-sensor core logger at 1-cm resolution at Brown University. We used core images and magnetic susceptibility measurements of the sediment to cross-correlate shared sediment features in MAHO08, MAHO19-3A, and MAHO19-1B and produce a composite stratigraphic succession that was a total of 426.5 cm long (Fig. 2). We sent a total of 16 radiocarbon samples of bulk sediment for accelerator mass spectrometry (AMS) radiocarbon dating at the National Ocean Sciences AMS (NOSAMS) facility at the Woods Hole Oceanographic Institution (Table 1). We used the Bacon age modeling program (Blaauw and Christen, 2011) using IntCal20 for the Northern Hemisphere (Reimer et al., 2020) to calculate an age-depth model for the composite core (Fig. 2). The inputs for this model included the radiocarbon sample depth, age, and uncertainty (Table 1). The resulting age-depth model suggests that the composite core from Lake Mahoma spans ~21.2 kyr.

3.2. brGDGT processing and analysis

We produced a record of MAAT using brGDGTs, which are

membrane lipids produced by bacteria that can be used for reconstructing temperature by quantifying their degree of branching (Weijers et al., 2007). Our record consists of 88 sediment samples with an average sampling resolution of ~200 years. We used procedures for lipid extraction and brGDGT analysis described in Hopmans et al. (2016) and Russell et al. (2018). We freeze-dried the sediment samples and homogenized each sample with a mortar and pestle. We then extracted the lipids using a DIONEX Accelerated Solvent Extractor with a solution of dichloromethane: methanol (DCM:MeOH, 9:1). We separated the lipid extract into neutral and acid fractions using aminopropylsilyl gel columns with DCM: isopropanol (DCM:IPA, 2:1) and ether: acetic acid (24:1), respectively, followed by methanol (MeOH) to remove any remaining polar compounds. We further separated the neutral fractions, which contained the brGDGTs, into four fractions using alumina gel columns with hexane, DCM, DCM:MeOH (1:1) and MeOH, with the brGDGTs eluting in the DCM:MeOH (1:1) fraction. We then dried this fraction under N₂ gas, dissolved it in a solution of hexane: IPA (99:1), and passed it through a 0.45 μm filter to remove particles. We measured the brGDGTs on an Agilent/Hewlett Packard 1100 series high-performance liquid chromatograph-mass spectrometer (HPLC-MS) using the chromatographic separation method presented in (Hopmans et al., 2016). This approach separates 5- and 6methyl brGDGT isomers, which is thought to produce more accurate paleotemperature reconstructions for brGDGTs from East African lake sediments (De Jonge et al., 2014; Russell et al., 2018). We performed analyses using selective ion monitoring (SIM) mode to track m/z 1302, 1300, 1298, 1296, 1292, 1050, 1048, 1046, 1036, 1034, 1032, 1022, 1020, 1018, and 744 (Table 2) and manually integrated the peak areas of the brGDGTs.

3.3. Lake Mahoma brGDGT temperature reconstruction

To determine the applicability of brGDGTs for temperature reconstruction at Lake Mahoma we calculated the Branched vs. Isoprenoidal Tetraether (BIT) index (Equation (1); Weijers et al., 2006), which represents the ratio of the sum of I, II, and III branched compounds to both branched and archaeal (IV) compounds, and can provide information about GDGT sources. If samples have BIT values near 1, the GDGTs are primarily sourced from bacteria, allowing for temperature reconstructions using brGDGTs. In contrast, samples with BIT values closer to zero are dominated by archaeal GDGT sources, which could limit the reliability of a

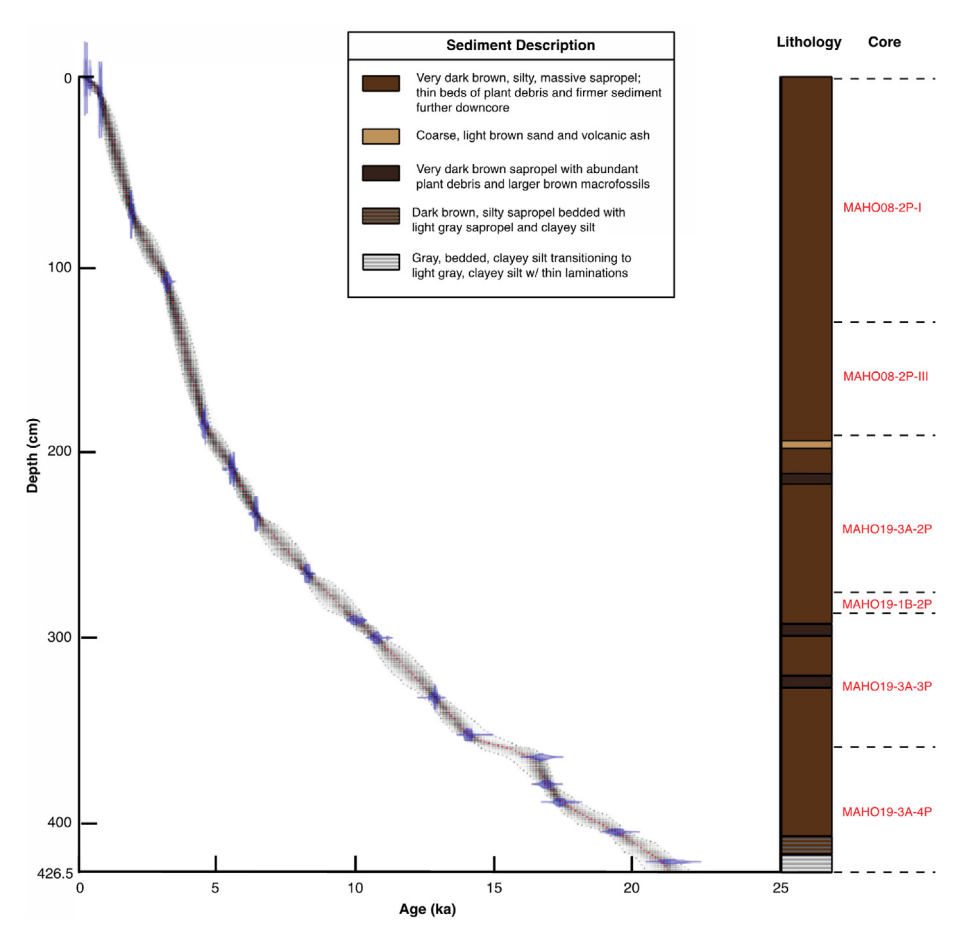


Fig. 2. Results from the Bacon age-depth model for Lake Mahoma (left), using IntCal20 for the Northern Hemisphere (Reimer et al., 2020) and the radiocarbon ages listed in Table 1. The red line is the ensemble mean estimate of age with depth and dotted lines indicate the 95% confidence interval. The blue points are the radiocarbon ages (from Table 1) with their calibrated ages and uncertainties. The uppermost blue point was manually set to an age of zero at 0 cm. We compare the age-depth model to the stratigraphic column and main lithologic features of the Lake Mahoma composite core (right). (For interpretation of the references to colour in this figure legend, the reader is referred to the Web version of this article.)

Table 1
Composite depths, radiocarbon ages and uncertainties, and median calibrated ages and uncertainties using the Northern Hemisphere IntCal20 calibration curve (Reimer et al., 2020) for each sample used to produce the age model.

Composite Depth (cm)	¹⁴ C Age (radiocarbon years)	¹⁴ C Age 1-σ error	Calibrated Age (years)	Calibrated Age 1-σ error
9.5	665	15	589	41
73	1,840	20	1,776	62
109	2,890	30	3,001	74
186	3,930	20	4,409	85
209.5	4,630	30	5,382	103
233.5	5,430	30	6,244	75
265.5	7,290	45	8,107	82
290.5	8,800	50	9,852	144
300	9,390	60	10,602	152
332	10,750	80	12,726	160
352	12,050	65	13,962	261
364	13,700	95	16,171	312
378.5	13,800	65	16,820	135
388	14,200	100	17,335	194
404	16,000	130	19,267	199
420	17,600	160	20,992	348

brGDGT-based temperature reconstruction (Hopmans et al., 2004; Weijers et al., 2007).

$$BIT = \frac{(I + II + III)}{(I + II + III + IV)}$$
 Equation 1

We also reconstructed the cyclization of branched tetraethers (CBT') using Equation (2) (Russell et al., 2018) to assess changes in brGDGT cyclization and Lake Mahoma pH over time, and the possible effect of this on our temperature reconstruction.

Table 2 Ions and structures of the brGDGTs (Weijers et al., 2007) used to produce the Lake Mahoma temperature record.

GDGT	Ions	Structures
Ia	1022	но _{То}
Ib	1020	но
Ic	1018	HO]
IIa	1036	но
IIb	1034	HO TO ON THE PART OF THE PART
IIc	1032	но <u>То</u>
IIIa	1050	но
IIIb	1048	HO TO ONLY ON THE PARTY OF THE
IIIc	1046	HO

$$\mathit{CBT'} = -\log\frac{(\mathit{Ic} + \mathit{IIa'} + \mathit{IIb'} + \mathit{IIc'} + \mathit{IIIa'} + \mathit{IIIb'} + \mathit{IIIc'})}{(\mathit{Ia} + \mathit{IIa} + \mathit{IIIa})}$$

Equation 2

To generate a reconstruction of MAAT at Lake Mahoma, we used the East African MBT'_{5Me} -based calibration (Equation (3); Russell et al., 2018), which calculates MAAT based on the index of methylation of branched tetraethers using only the 5-methyl isomers (MBT'_{5Me}).

$$MAAT = -1.21 + 32.42 \times MBT_{5Me}$$
 Equation 3

MBT'_{5Me} quantifies the degree of brGDGT branching, which is a physiological response to maintain membrane viscosity under changing temperatures. The East African MBT'_{5Me} calibration regresses MAAT onto the MBT'_{5Me} index (Russell et al., 2018). Previous work using East African lake sediments shows that this calibration has yielded temperature reconstructions that more closely fit modern East African MAAT values than brGDGT calibrations based on soil and peat, which generally produce a 'cold bias' relative to observed present-day temperatures (Loomis et al., 2011; Russell et al., 2018). To assess the applicability of this calibration, we calculated the fractional abundances of each brGDGT isomer in the Lake Mahoma samples, as well as the sum of the tetra-, penta-, and hexamethylated brGDGTs, to determine whether they fall within the typical ranges for East African lake sediments, and compared temperatures estimated from the uppermost sediment to presentday observations.

We calculated the uncertainty of the Lake Mahoma temperature reconstruction by incorporating the regression error associated with the MBT' $_{5\text{Me}}$ calibration and the analytical error associated with laboratory measurements. This method of calculating the

temperature error is similar to approaches used in other studies (e.g., Loomis et al., 2012) to calculate the uncertainty associated with GDGT-based temperature reconstructions.

3.4. East African temperature comparisons

We compare our new record to previously published GDGTbased temperature reconstructions from East Africa to evaluate large-scale temperature changes including elevation-dependent warming. Previous brGDGT-based temperature reconstructions from Lake Rutundu (Loomis et al., 2017) and Sacred Lake (Loomis et al., 2012) were calibrated using an East African lake calibration from Loomis et al. (2012), measured using a HPLC-MS procedure that did not separate 5- and 6-methyl brGDGT isomers. Temperature reconstructions from Lake Tanganyika (Tierney et al., 2008) and Lake Malawi (Powers et al., 2005) are based on the tetraether index of 86 carbon atoms (TEX₈₆), which is a GDGT-based temperature proxy that quantifies the relative degree of cyclization of isoprenoidal GDGTs, rather than the degree of branching as in brGDGT reconstructions. For these latter two records, we calculated temperature using the linear calibration of TEX₈₆ to observed temperature described in Loomis et al. (2017). Because the composite Lake Tanganyika temperature reconstruction was produced from one short core and one deep sediment core, we added a correction of 0.011 to the TEX_{86} values of the surface sediment core prior to performing the temperature calibration, as described in Loomis et al. (2017), to account for the offset in TEX₈₆ between these two core sites. Due to the corrections we performed on the Lake Tanganyika and Lake Malawi records, the temperatures we report for these two sites are different from those reported in the original papers. However, the differences in temperature are minor (~3.6 °C on average for Lake Tanganyika and ~1 °C on average for Lake Malawi) and the corrections allowed us to compare these TEX₈₆-based temperature reconstructions to brGDGT-based temperature reconstructions.

4. Results and discussion

4.1. Lake Mahoma brGDGT indices and temperature reconstruction

The fractional abundances of brGDGTs in the Lake Mahoma sediments are similar to the average fractional abundances of East African lake surface sediments (Fig. 3A; Russell et al., 2018). Additionally, the summed tetra-, penta-, and hexamethylated brGDGTs in Lake Mahoma are within the range of values for East African lake surface sediments (Fig. 3B; Russell et al., 2018). These similarities indicate that the brGDGTs in the Lake Mahoma sediment cores are consistent with brGDGTs sourced from other East African lake sediments in the regional calibration and suggest that we can use temperature calibrations specific for East African lake sediments to interpret past changes in temperature at Lake Mahoma.

The average CBT' for Lake Mahoma over the past 21.2 kyr was 0.77, with a standard deviation of 0.26. Between the LGM and late Holocene, CBT' varied from 0.17 to 1.31, with an average value of 0.38 during the LGM and an average value of 1.08 during the late Holocene (Fig. 4A). CBT' gradually increases between the LGM and present, consistent with a long-term decrease in lake pH. Existing calibrations of CBT' to pH in East African lakes are highly uncertain (Russell et al., 2018), so we do not estimate pH values. However, we would expect the pH of Lake Mahoma water to decrease over this time as the lake and its catchment transitioned from a freshly deglaciated landscape following the LGM to the oligotrophic and acidic lake rich in dissolved organic carbon that exists today. Similar shifts have been observed in the Arctic (Engstrom et al., 2000), and modern Rwenzori lakes exhibit strong gradients in pH and

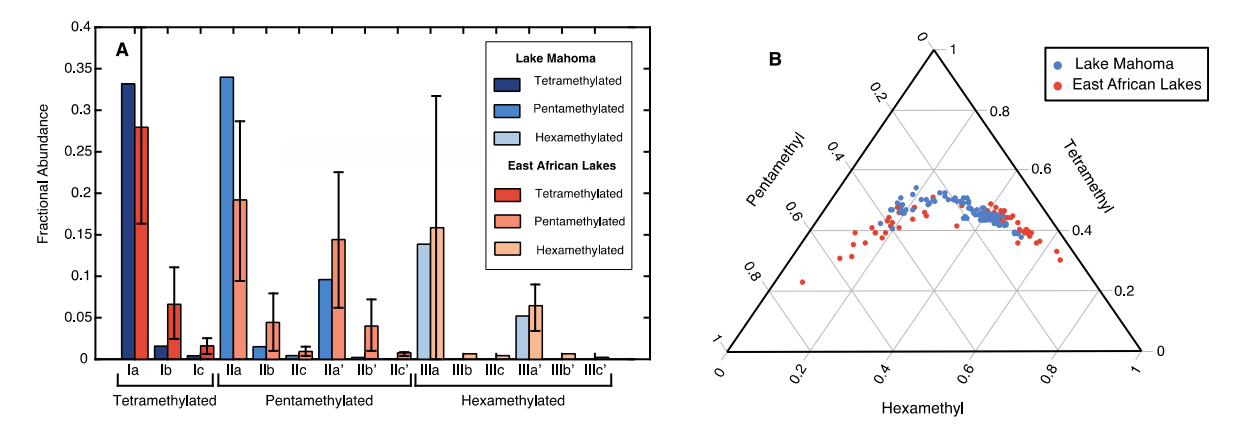


Fig. 3. A) Average fractional abundances of the individual brGDGTs in Lake Mahoma (shades of blue) and other East African lake surface sediments (shades of orange; Russell et al., 2018) with error bars. B) The fractional abundances of summed tetramethylated, pentamethylated, and hexamethylated brGDGTs in Lake Mahoma (blue) are plotted versus the summed values from East African lakes (orange; Russell et al., 2018). (For interpretation of the references to colour in this figure legend, the reader is referred to the Web version of this article.)

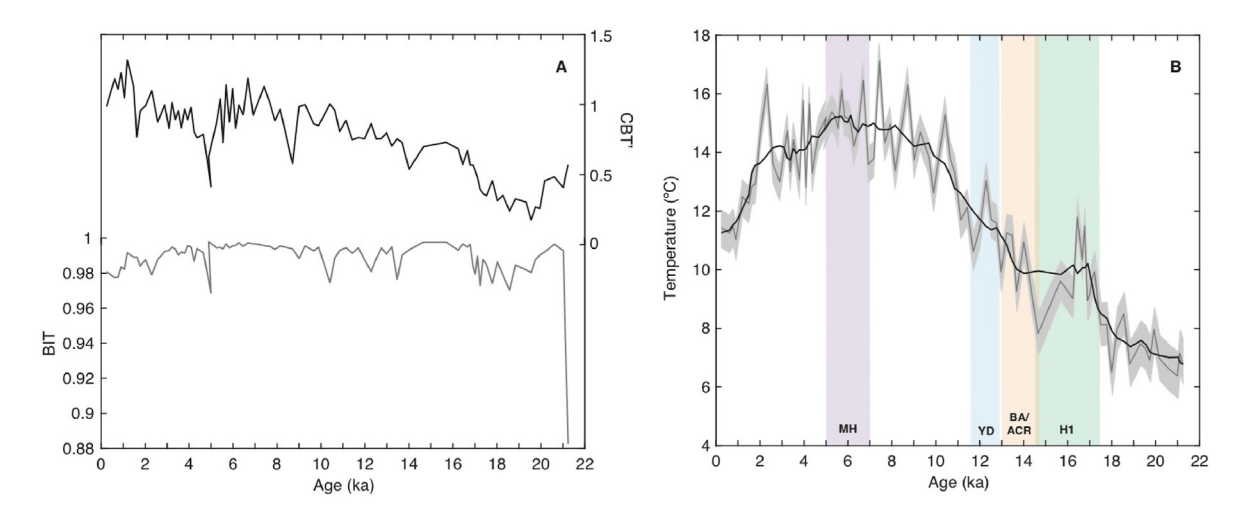


Fig. 4. A) Reconstruction of Lake Mahoma CBT' (black line) and BIT index values (gray line) since the LGM. B) brGDCT-based temperature reconstruction using the East African temperature calibration (gray line; "unsmoothed"), the running average (black line; "smoothed") and 2-sigma uncertainty (gray shaded). We calculated the running average using the "movmean" function in Matlab and calculated the mean over a sliding window of 7 adjacent temperatures. The specific climate events and time periods discussed in the text are shaded: middle Holocene (MH; 7–5 ka; purple), Younger Dryas (YD; 12.9–11.6 ka; blue), Bolling-Allerod (BA; 14.7–13 ka; yellow), Antarctic Cold Reversal (ACR; 14.7–13 ka; yellow) and Heinrich Stadial 1 (H1; 17.5–14.5 ka; green). The small, dark shaded area between 14.7–14.5 ka is due to the overlap in timing between the ACR and BA with H1. (For interpretation of the references to colour in this figure legend, the reader is referred to the Web version of this article.)

dissolved organic carbon content depending on their proximity to glaciers (Eggermont et al., 2007; Engstrom et al., 2000).

There is a relatively weak correlation between CBT' and temperature ($r^2 = 0.51$); however, trends in CBT' and temperature are visually distinct (Fig. 4A and B), suggesting that the pH evolution of Lake Mahoma had little influence on reconstructed temperature. Additionally, the BIT index for Lake Mahoma brGDGTs was nearly constant over the past 21.2 kyr with an average BIT value of 0.987 and a standard deviation of 0.014 (Fig. 4A). This consistency over time of a BIT value close to 1 suggests that bacteria were the primary sources of GDGTs in Lake Mahoma. The two outlier values resulting in the decrease in BIT at ~21 kyr are likely due to the fact that the two samples from furthest downcore were taken from a thin clave silt bed at the base of the core (Fig. 2), interpreted to reflect glacially-derived clastic sediment. The other samples were taken from the overlying lacustrine sapropels (Fig. 2). There is no correlation between temperature and BIT when excluding the two outliers ($r^2 = 0.08$), suggesting that our temperature values are not affected by changes in the organisms producing the brGDGTs.

Lastly, core-top temperatures estimated from Equation (3) are ~11.4 $^{\circ}$ C, which is very close to the modern observed MAAT of 10 $^{\circ}$ C. Overall, these results highlight the strong potential for brGDGTs to register past changes in MAAT at Lake Mahoma.

4.2. Local Rwenzori temperature change

The brGDGT-based temperature reconstruction from Lake Mahoma is marked by warming during the last global deglaciation, a temperature maximum during the mid-Holocene, and cooling toward the present. The average 2-sigma error associated with the temperature reconstruction is ~0.65 °C (Fig. 4B). The "unsmoothed" record (Fig. 4B, gray line) exhibits substantial sub-millennial variability that is difficult to interpret given the relatively low sampling resolution (200–300 years). Thus, our discussion focuses principally on the "smoothed" trend (Fig. 4B, black line), though we use the "unsmoothed" record (Fig. 4B, gray line) to evaluate the timing of changes.

Our new temperature record from the Rwenzori mountains

shows a relatively constant temperature during the last millennium of the LGM, with an average MAAT of ~7 °C (Fig. 4B). There is a slight increase in temperature beginning at ~20 ka, followed by more rapid warming beginning at 18.5 ka in the smoothed record and 18 ka in the unsmoothed record. This rapid warming is followed by a pause in warming in the smoothed record from ~16.4 to 14 ka, and a temporary return to cooler temperatures in the unsmoothed record from ~16 to 14.6 ka (Fig. 4B). This interval coincides with the latter phases of Heinrich Stadial 1 (H1; 17.5-14.5 ka; Hodell et al., 2017), a millennial-scale, Northern Hemisphere (NH) high-latitude cooling event (e.g., Hodell et al., 2017; Stager et al., 2011). In the Lake Mahoma temperature record, warming recommenced ~14.6 ka in the unsmoothed record (~14 ka in the smoothed record), near the onset of the Bølling-Allerød (BA; 14.7-13 ka; Pedro et al., 2011), a millennial-scale, NH high-latitude warming event, and the Antarctic Cold Reversal (ACR; 14.7-13 ka; Pedro et al., 2016), a millennial-scale, Southern Hemisphere (SH) high-latitude cooling event. Although these features in our record could suggest a teleconnection between Rwenzori and northern high-latitude temperature changes, we do not observe significant cooling during the Younger Dryas (YD; 12.9-11.6 ka; Svensson et al., 2008), another millennial-scale, NH high-latitude cooling event. That said, the sampling resolution of our record during the deglaciation is relatively low (approximately one sample per 300 years) and the temperature record has high sample-to-sample variability, limiting our ability to evaluate millennial-scale events.

The warming beginning between 14.6–14 ka in both the smoothed and unsmoothed records continues until the middle Holocene (Fig. 4B), culminating with the warmest temperatures in the Lake Mahoma record occurring during the middle Holocene (7–5 ka) when MAAT reached ~14.8 °C (Fig. 4B). Temperatures begin to cool at ~5 ka and reach an average temperature of ~11.9 °C between 2-0 ka, and a near-modern (0.22 ka; the age of the youngest sample in the record) temperature of ~11.4 °C. This is similar to modern observed temperatures at Lake Mahoma (10 °C; Eggermont et al., 2007; Loomis et al., 2017; Mackay et al., 2021). The small difference in modern temperature is likely due to small sitespecific biases in the brGDGTs or observed temperatures.

There are striking similarities between our temperature reconstruction and ¹⁰Be exposure ages of glacial moraines from the Rwenzori Mountains, which document the deglacial retreat and inferred late Holocene readvance of Rwenzori glaciers (Jackson et al., 2019, 2020; Vickers et al., 2021). The ¹⁰Be ages of glacial moraines document the last time at which a glacier extended to a given elevation and can therefore provide a record of glacial retreat and inferred warming. Both the Lake Mahoma temperature record and the Rwenzori glacial moraine ¹⁰Be ages suggest a similar timing of the onset of warming and glacial retreat, with a slight warming and glacial retreat beginning by ~20 ka, followed by a larger increase in deglacial warming and glacial retreat ~18.5-18 ka (Fig. 5A). Specifically, the ¹⁰Be moraine exposure ages in the Mubuku and Bujuku Valleys, some of which are adjacent to Lake Mahoma, indicate that from ~21.5 ka to ~18.7 ka, the glaciers retreated upslope by ~250 m in elevation over ~2,800 years, whereas from ~18.7 ka to ~17.9 ka, the moraine ages suggest that the glaciers retreated by ~560 m in elevation over only ~880 years. During H1 and the ACR, the ¹⁰Be moraine ages in the Bujuku Valley record a pause in glacier recession, consistent with the pause in warming in the smoothed Lake Mahoma temperature record and temporary cooling in the unsmoothed record (Fig. 5A). Additionally, the ¹⁰Be ages of moraines in the Bujuku and Nyamugasani Valleys suggest that glaciers may have retreated during the YD, which is in agreement with the absence of cooling during the YD in the Lake Mahoma temperature record (Fig. 5A). Finally, during the late Holocene, following the period of maximum warming in the Lake

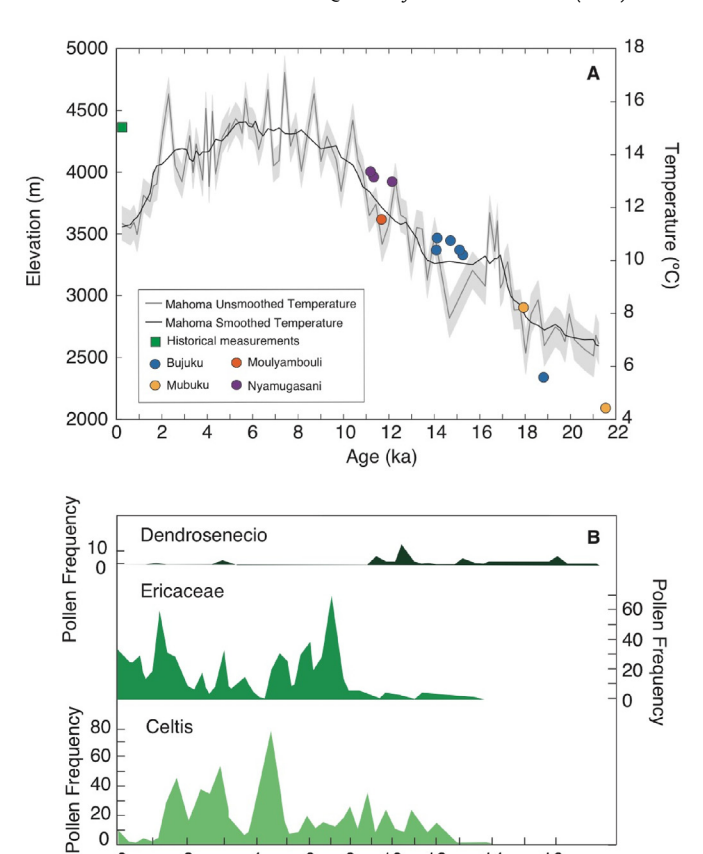


Fig. 5. A) Lake Mahoma brGDGT-based temperature reconstruction (gray line; "unsmoothed"), running average (black line; "smoothed") and 2-sigma uncertainty (gray shaded) plotted versus the arithmetic mean of glacial moraine ¹⁰Be ages (Jackson et al., 2019, 2020) from four valleys in the Rwenzori Mountains (Bujuku, blue; Mubuku, yellow; Moulyambouli, orange; Nyamugasani, purple). The elevations associated with the glacial moraine 10Be ages are the elevations from which samples were taken (i.e., elevations of the moraines). The green square indicates the average age and elevation of historical measurements of Rwenzori ice margins in 1958 (Whittow et al., 1963). B) Pollen reconstructions from Lake Mahoma (Livingstone, 1967). The pollen frequency refers to the number of each pollen type per volume of sediment. The three pollen types shown are from plants that grow at different elevations in the Rwenzori Mountains today: dendrosenecio from high-elevation plants, ericaceae from midelevation plants, and celtis from low-elevation plants. (For interpretation of the references to colour in this figure legend, the reader is referred to the Web version of this article.)

10 12

Age (radiocarbon kyr)

14

16

80

60

40

20

0

Celtis

Mahoma temperature record, historical measurements of Rwenzori ice margins suggest that the glaciers advanced, which coincides with late Holocene cooling in the Lake Mahoma temperature record (Fig. 5A). A similar cooling and increased glacial extent during the late Holocene is also recorded in the Quelccaya Ice Cap (Vickers et al., 2021), possibly indicating a pan-tropical cooling event during the late Holocene. Overall, both the Lake Mahoma temperature and Rwenzori glacial moraine records register similar times and signs of change in local temperature during the last deglaciation and Holocene. We also observe similar trends in the Lake Mahoma temperature record and the ¹⁰Be exposure ages of Rwenzori glacial moraines when we evaluate glacier retreat in terms of horizontal distance, rather than elevation (Supplementary Figure 1).

The Lake Mahoma temperature record and the glacial moraine ¹⁰Be ages also imply considerable warming during the middle Holocene (Fig. 5A). The Lake Mahoma record suggests temperatures averaged ~3.4 °C warmer during the middle Holocene than the present day, and the absence of glacial moraines of middle-Holocene age suggests that glaciers were inboard of their latest Holocene extents during this time. Holocene glacial extent histories based on *in situ* ¹⁰Be and ¹⁴C data derived from near the Rwenzori summits indicate prolonged exposure (i.e., glacial retreat to near summit elevations) during the early to middle Holocene (Vickers et al., 2021). Additionally, a two-dimensional ice-flow and mass-balance glacier model forced with alpine temperature reconstructions from Mt. Kenya (Loomis et al., 2017) predicts that the Rwenzori Mountains were ice-free for most of the early to middle Holocene (Doughty et al., 2020), further supporting the temperature estimates from Lake Mahoma.

To further investigate this relationship between the ¹⁰Be moraine ages and Lake Mahoma temperatures during the middle Holocene, we used the Lake Mahoma temperature record to estimate changes in the zero-degree isotherm (i.e., the altitude at which the temperature reaches 0 °C) using two approaches: one by calculating a regional middle-Holocene air-temperature profile based on existing temperature records from tropical East Africa, and the other by calculating a local middle-Holocene air temperature profile using the middle-Holocene temperature anomaly from the Lake Mahoma record. For the first approach, we calculated a middle-Holocene (5–7 ka) air temperature profile using a regional middle-Holocene temperature lapse rate of -5.6 °C/km (determined using the calculations described in Section 4.4) and a middle-Holocene sea level surface temperature of 27.72 °C, based on a modern sea level surface temperature of 27.5 °C (Loomis et al., 2017) and an average tropical SST warming of 0.22 °C during the middle-Holocene relative to the present (Kaufman et al., 2020). Based on these calculations, the zero-degree isotherm of the Rwenzori Mountains would have been located at ~4.950 m asl during this time. Given that the highest point in the Rwenzori is Margherita Peak (5,109 m asl), a zero-degree isotherm of ~4,950 m asl suggests temperatures were too warm to support glaciers for prolonged periods in all but the highest summits during this time. For the second approach, we calculated a modern air temperature profile using a modern lapse rate of -5.8 °C/km (Loomis et al., 2017), a modern sea level surface temperature of 27.5 °C (Loomis et al., 2017), and added the present to middle-Holocene temperature anomaly observed in the Lake Mahoma record (~3.4 °C) to create a local middle-Holocene temperature profile, specific to the Rwenzori Mountains. Based on these calculations, the zero-degree isotherm of the Rwenzori Mountains would have been located at ~5,260 m asl during the mid-Holocene. This elevation is ~150 m higher than Margherita Peak, suggesting complete deglaciation during this time based on this calculation. Regardless of the method used to calculate the zero-degree isotherm, our results suggest the degree of warming observed over this interval resulted in little to no glaciated area in the Rwenzori during the middle Holocene. In addition, glacier modeling by Doughty et al. (2020) indicates a middle-Holocene zero-degree isotherm at 5,020 m asl, similar to the results of both of our calculations and further supporting the argument of minimal glaciation in the Rwenzori during the middle Holocene.

The similar timing of warming and cooling documented by the Lake Mahoma temperature record and the fluctuations of Rwenzori glaciers highlights the importance of temperature change to these high-elevation tropical glaciers. Previous work suggests that glacier extent in the Rwenzori is primarily controlled by variations in incoming shortwave radiation driven by changes in cloudiness and relative humidity, such that a drier, less humid climate would result in fewer clouds, increased shortwave radiation, and glacial ablation (Mölg et al., 2003). Our data cannot be used to directly test this hypothesis, but the glacial moraine data from the Rwenzori suggest that glaciers advanced during the late-Holocene relative to the mid-Holocene (Fig. 5A), during which time the climate in tropical East Africa became drier (e.g., Gasse, 2000; Tierney et al., 2008), but

also cooler, as observed in our temperature record. Therefore, our results suggest that although humidity may partially contribute to fluctuations in Rwenzori glaciers, temperature is the dominant control on Rwenzori glacial extent on orbital timescales. This is consistent with previous work suggesting that tropical glaciers located closer to the equator, such as those in the Rwenzori, are predominantly controlled by temperature, whereas tropical glaciers in the outer tropics are primarily controlled by humidity (Favier et al., 2004; Groos et al., 2021).

In addition to our temperature record and the existing glacial moraine 10Be ages recording glacial retreat, fossil pollen records from lake sediment cores in the Rwenzori Mountains suggest that changes in temperature since the LGM played a key role in large local changes in vegetation over this time. Although the fossil pollen records are from sediment cores previously recovered from Lake Mahoma (Livingstone, 1962, 1967), these cores contain basal silt similar to that present in our cores, suggesting that the cores record the same time span. The vegetation reconstructions from these previous cores show a high abundance of shrub and herb pollen during the LGM, suggesting an Afroalpine environment at the site during this time and possibly reflecting a cool, dry climate (Fig. 5B). This was followed by the presence of alpine taxon (Dendrosenecio) along with the appearance of Ericaceous vegetation during the deglaciation, as lower-elevation taxa moved upslope (Fig. 5B). For example, Dendrosenecio, which is located at high elevations in the Rwenzori today, was present around Lake Mahoma during the LGM at a time when the brGDGT temperature reconstruction shows the coolest temperatures (~7.1 °C). During the early Holocene, when the Lake Mahoma brGDGT reconstruction registers increased warming, Ericaceous pollen became the most abundant pollen taxon at Lake Mahoma, likely representing the dominance of vegetation associated with the Ericaceous belt present at midelevations today. During the middle Holocene, Livingstone (1967) observed an increase in montane and submontane forest pollen taxa (e.g., Celtis) as Ericaceous pollen declined. Livingstone (1967) tentatively interpreted this transition as driven by either climate or human impacts; however, coupling the fossil pollen records with the Lake Mahoma temperature record confirms that considerable warming was associated with the upslope appearance of these lower elevation montane and submontane forest taxa. During the late Holocene, Ericaceous pollen reappears, coincident with a cooling trend in the Lake Mahoma brGDGT temperature record, suggesting a lowering of this vegetation belt from higher altitudes.

Together, these results highlight the dynamism of Rwenzori glaciers, ecosystems, and temperatures. The sensitivity of both Rwenzori glaciers and vegetation to local temperature change has important implications for understanding the future impacts of climate warming and impending deglaciation in local environments. Our results suggest that the glacial and environmental response to middle-Holocene warming in the Rwenzori could serve as an analog for future changes.

4.3. Regional tropical East African temperature change

GDGT-based temperature reconstructions from other East African lakes generally suggest a similar timing of deglacial warming as seen in the Lake Mahoma record (Fig. 6). Temperature reconstructions from Sacred Lake (Loomis et al., 2012), Lake Tanganyika (Tierney et al., 2008), and Lake Malawi (Powers et al., 2005) all show a gradual warming beginning ~21 ka followed by a larger increase in the rate of warming at ~18.3 ka, similar to the trends seen at Lake Mahoma (Fig. 6). This initial warming at ~21 ka is roughly synchronous with the onset of high-latitude deglaciation but precedes changes in global GHG concentrations and radiative forcing in the tropics, suggesting links between high and low-

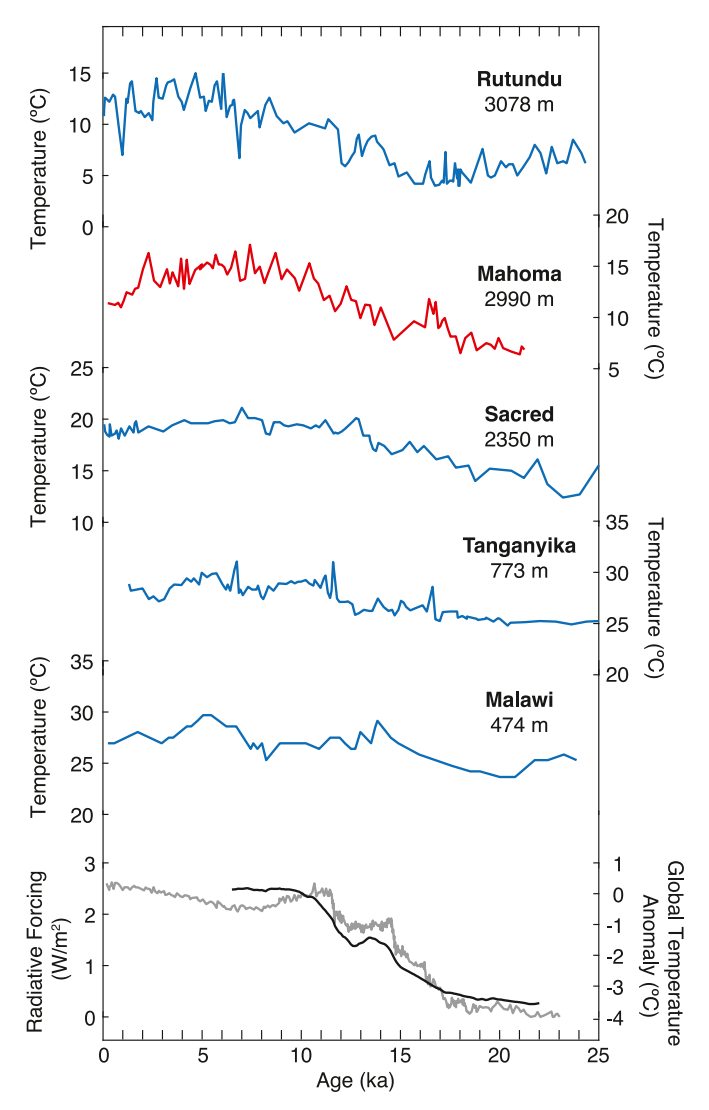


Fig. 6. GDGT-based temperature reconstructions from East African lakes of varying elevations. Records are plotted top to bottom from highest to lowest elevation: Lake Rutundu (Loomis et al., 2017), Lake Mahoma (red; this study), Sacred Lake (Loomis et al., 2012), Lake Tanganyika (Tierney et al., 2008), and Lake Malawi (Powers et al., 2005). All records are plotted on the same range of temperatures to highlight the difference in amplitude of temperature change at various elevations. Temperature records are compared to global temperature anomalies (black line; Shakun et al., 2012) and radiative forcing from greenhouse gases (gray line) calculated from changes in the concentration of CO₂ from WAIS (Marcott et al., 2014) and EPICA Dome C (Monnin et al., 2004), CH₄ (Brook et al., 1996), and N₂O (Schilt et al., 2010). (For interpretation of the references to colour in this figure legend, the reader is referred to the Web version of this article.)

latitude temperature changes at this time (Jackson et al., 2019). More rapid warming in these records by ~18.3 ka is consistent with the timing of increased global temperatures and radiative forcing from GHGs (Fig. 6), suggesting that increased radiative forcing from GHGs may have contributed to regional deglacial warming in East Africa. In this context, the mid-Holocene warming recorded at Lake Mahoma is enigmatic, as it occurs near a minimum in changes in radiative forcing during the Holocene. Nevertheless, the Lake Mahoma reconstruction, combined with glacial extent and palynological records, highlights the significance of the observed mid-Holocene warming in the temperature record. Additionally, lake surface temperature records from Lakes Tanganyika, Malawi, Turkana, and Sacred Lake record maximum warming at ~5 ka, similar to the Lake Mahoma record (Berke et al., 2012b). Berke et al.

(2012b) suggested that this warming was driven by the sensitivity of lake energy budgets to maximum local insolation from September to November; however, the observation of this feature in lacustrine, glaciological, and vegetation records suggests other processes are likely important. At present, this event requires further investigation.

The temperature reconstruction from Lake Rutundu (Loomis et al., 2017), a site on Mt. Kenya in East Africa at an elevation similar to Lake Mahoma, is anomalous in that it records a slight cooling trend in temperature from the LGM to ~16 ka, at which time temperatures began to warm (Fig. 6). The Lake Mahoma record does not replicate this trend; however, the temperature changes observed at Lake Mahoma are very similar to the changes observed at Sacred Lake, located close to Lake Rutundu on Mt. Kenya and the only other montane record currently available from tropical East Africa (Loomis et al., 2012). This suggests that the Lake Rutundu temperature record may have recorded local changes in temperature specific to the Lake Rutundu catchment. Overall, the coherence in timing between deglacial warming in the Lake Mahoma temperature record, other East African temperature records, radiative forcing and global temperature, confirms that deglacial warming in the low latitudes was driven by a combination of high-latitude processes and radiative forcing from GHGs (Jackson et al., 2019; Shakun et al., 2012).

4.4. Implications for regional lapse rate changes

Despite the similarities in the timing of transitions in the East African temperature records, there are differences in the magnitude of warming from the LGM to late Holocene among the GDGT-based temperature reconstructions in East Africa. Overall, the magnitude of temperature change was larger at higher elevation sites (i.e., Lake Rutundu and Lake Mahoma) than at lower elevation sites (i.e., Lake Tanganyika and Lake Malawi). The temperature reconstructions from Lake Rutundu (3,078 m asl) and Lake Mahoma (2,990 m asl) record an LGM (19.5–22.5 ka) to late Holocene (0–2 ka) warming of ~5.7 °C and ~4.9 °C, respectively. In contrast, the lower elevation temperature reconstructions from Lake Tanganyika (773 m asl) and Lake Malawi (474 m asl) each only record a warming of ~3.3 °C and ~2.8 °C, respectively, similar to the amplitude of warming from fossil pollen (Bonnefille et al., 1990). Sacred Lake, located at 2,350 m asl, has an intermediate level of warming of ~4.0 °C. The magnitude of LGM to late Holocene warming observed in the Lake Mahoma record supports results from Loomis et al. (2017) that showed higher elevation regions of tropical East Africa experienced a larger magnitude of cooling than lower elevation sites during the LGM and that, regionally, the tropical temperature lapse rate was steeper during the LGM relative to the late Holocene.

The temperature changes at Lake Mahoma are slightly smaller than those at Lake Rutundu, and we therefore calculated a revised lapse rate estimate for the LGM. We used a modern air-temperature profile based on a modern lapse rate of -5.8 °C/km (Loomis et al., 2017) and a modern sea level surface temperature of 27.5 °C (Loomis et al., 2017), then subtracted the LGM to late Holocene anomalies for each tropical East African site mentioned above from the modern air temperature at the elevation of each site. For the change in SST from the LGM to late Holocene, we used an anomaly of 2.03 °C, which is the average change in temperature recorded in proxy-based SST reconstructions from the Western Indian Ocean (Tierney et al., 2020). We plotted these calculated LGM temperatures versus the LGM elevations for each site (Fig. 7), which take into account lake-level and sea-level changes during the LGM, as described in Loomis et al. (2017), and took the slope of the linear regression through these points. Doing so, we find that the lapse rate was -6.4 °C/km during the LGM (Fig. 7). This updated LGM

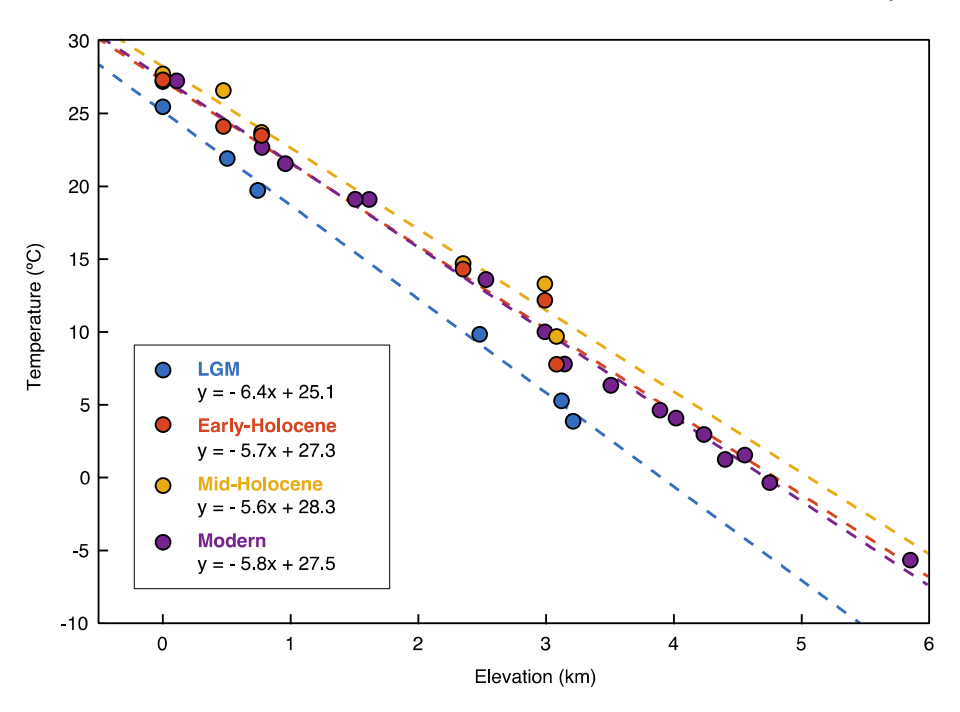


Fig. 7. The elevation of each site (Lake Rutundu, Lake Mahoma, Sacred Lake, Lake Tanganyika and Lake Malawi) plotted versus the calculated temperature from the proxy reconstructions for each site (as described in the text) during the LGM (19.5–22.5 ka; blue), early-Holocene (9–11 ka; orange), and mid-Holocene (5–7 ka; yellow). The LGM temperatures are plotted versus the LGM elevations for each site. The SSTs for each time interval were calculated as described in the text. The modern temperature data (purple), is derived from reanalysis data and temperature loggers in the Rwenzori Mountains (Loomis et al., 2017). The slopes of the linear regressions through the data points for each time interval (dashed lines) suggest a lapse rate of -6.4 °C/km during the LGM, -5.7 °C/km during the early-Holocene, -5.6 °C/km during the mid-Holocene, and -5.8 °C/km in the modern. (For interpretation of the references to colour in this figure legend, the reader is referred to the Web version of this article.)

lapse rate is similar to, but shallower than, the LGM lapse rate of $-6.7\,^{\circ}\text{C/km}$ as calculated by Loomis et al. (2017). This reduction makes our revised lapse rate estimate more similar to, but still steeper than, the tropical lapse rates simulated by paleoclimate models for the LGM (Loomis et al., 2017). Overall, our results suggest that the temperature lapse rate in tropical East Africa was steeper during the LGM than it was during the late Holocene and today.

Although there are other periods of cooler than modern temperatures since the LGM (e.g., H1, the ACR and YD) observed in some tropical East African temperature records, a low sampling resolution in many of these records makes it is difficult to determine conclusively the extent to which the temperature lapse rate in tropical East Africa changed during these millennial-scale events. Additionally, there are spatially inconsistent features in the East African temperature records during H1, the ACR and the YD that present challenges for calculating the lapse rate. For example, the temperature reconstruction from Lake Rutundu records cooling during the first half of the YD (Fig. 6), yet neither the record from Lake Mahoma nor Lake Tanganyika (Tierney et al., 2008), Sacred Lake (Loomis et al., 2012) or Lake Victoria (Berke et al., 2012a) record any significant cooling. Similarly, although minimum temperatures are recorded during H1 in the Lake Rutundu temperature record, this is a unique feature at this site and is not present in either our Lake Mahoma record or other temperature records from the region (Fig. 6).

In contrast, existing reconstructions of Holocene temperature consistently record mid-Holocene warming. To evaluate potential lapse-rate changes at this time, we calculated the early-Holocene (9–11 ka) and middle-Holocene (5–7 ka) lapse rates in this region using the same methods described for the LGM lapse rate calculations. For the early-Holocene and middle-Holocene SST anomalies, we used $-0.19~\rm ^{\circ}C$ and $0.22~\rm ^{\circ}C$, respectively, which are

the average change in SST between each time period and the late Holocene for regions between 30°N and 30°S (Kaufman et al., 2020). These calculations yielded a tropical East African lapse rate of -5.7 °C/km during the early Holocene and -5.6 °C/km during the middle Holocene (Fig. 7). Calculations using average temperature anomalies for the early and middle Holocene derived from local SST records (Rippert et al., 2015; Romahn et al., 2014) give the same lapse rates for these time periods. Although these lapse rate calculations are slightly shallower than the modern lapse rate of -5.8 °C/km, they are within the range of error for these calculations and suggest that there was little to no change in the temperature lapse rate during the Holocene.

We recognize that our lapse rate calculations reflect local environmental lapse rates rather than free air lapse rates, and therefore may reflect influences of along-slope local processes. However, the present-day environmental lapse rate calculated from observational data in the Rwenzori Mountains is nearly identical to the modern free air lapse rate from reanalysis data in tropical East Africa, and our temperature reconstructions from Lake Mahoma are generally similar to records from Mt. Kenya, nearly 1,000 km to the east. Therefore, we assume that our lapse rate reconstructions can be used to assess larger scale changes in the free air lapse rates of the tropics.

The tropical lapse rate is directly controlled by tropical SSTs and atmospheric water vapor content (e.g., Kageyama et al., 2005) and, thus, a combination of cooler tropical SSTs and lower atmospheric humidity during the LGM likely resulted in a steeper temperature lapse rate in the African tropics during this time. Previous work suggests that the tropical SSTs were 2–4 °C cooler during the LGM than today (Loomis et al., 2017; Tripati et al., 2014) but may have been as large as 3.7–4.2 °C cooler (Tierney et al., 2020). Since atmospheric water vapor is closely related to temperature via the temperature dependence of saturation vapor pressure, cooler

tropical SSTs during the LGM likely resulted in lower atmospheric humidity and a drier climate, therefore resulting in a steeper temperature lapse rate (Kageyama et al., 2005). In contrast, tropical SSTs exhibit much smaller temperature changes during the Holocene, which was generally a humid period relative to the LGM (e.g., Gasse, 2000; Otto-Bliesner et al., 2014; Tierney et al., 2008).

A steeper temperature lapse rate in the tropics during the LGM and minimal to no change in the lapse rate during the Holocene has important implications for understanding large-scale climate feedbacks that influence temperature sensitivity. An increase in temperature from the LGM to Holocene contributed to a shoaling of the temperature lapse rate due to the direct effect of SST (Kageyama et al., 2005), as well as increased atmospheric water vapor and relative humidity (Bony et al., 2006; Held and Soden, 2006). However, the lack of a significant change in the lapse rate during the Holocene suggests that although high-elevation warming occurred during this time, atmospheric water vapor and relative humidity were likely more stable than during the deglacial transition from the LGM to Holocene. We would expect this observed stability in the tropical lapse rate during the Holocene given the relative stability of tropical SST during this time (Kaufman et al., 2020).

5. Conclusions

The brGDGT-based temperature reconstruction from Lake Mahoma, located at a high elevation in tropical East Africa, records a large deglacial warming and maximum temperatures during the middle Holocene. The timing of temperature changes seen in the Lake Mahoma record corresponds with the timing of changes in glacial extents and pollen in the Rwenzori Mountains, suggesting that the record accurately records the timing and sign of local and regional changes in temperature. Additionally, the Lake Mahoma temperature reconstruction records a large magnitude of LGM to late-Holocene warming, similar to that observed in high-elevation temperature records from Mount Kenya. Together, these results indicate that high-elevation sites in tropical East Africa warmed more from the LGM to present than lower elevation sites in this region, providing evidence that the tropical temperature lapse rate was steeper during the LGM than it is today.

The transition from a steeper temperature lapse rate during the LGM to a shallower temperature lapse rate during the Holocene likely had significant environmental impacts on tropical mountains, such as shifts in montane vegetation belts and glacial retreat. Temperature changes at Lake Mahoma correspond to observations of regional vegetation migration up and downslope, as well as glacial retreat and advance, therefore pointing to the strong impact of warming signals on montane environments and glaciers. This supports the idea that shoaling of the tropical temperature lapse rate in the future will continue to impact the environments and glaciers of high-elevation mountains in the tropics. Understanding how the tropical temperature lapse rate has changed since the LGM has important implications for modeling large scale climate feedbacks that influence temperature sensitivity, such as water vapor, and can improve projections of future climate change in these sensitive tropical mountains.

Author contributions

Sloane Garelick: Writing — original draft, Conceptualization, Formal analysis, Investigation, Resources. **James Russell**: Writing — review & editing, Conceptualization, Funding acquisition, Resources. **Adin Richards**: Writing — review & editing, Investigation. **Jamila Smith**: Writing — review & editing, Investigation. **Meredith Kelly**: Writing — review & editing, Conceptualization, Funding

acquisition. **Nathan Anderson**: Writing — review & editing. **Margaret Jackson**: Writing — review & editing. **Alice Doughty**: Writing — review & editing. **Bob Nakileza**: Writing — review & editing, Resources. **Sarah Ivory**: Writing — review & editing. **Sylvia Dee**: Formal analysis.**Charlie Marshall**: Formal analysis

Declaration of competing interest

The authors declare that they have no known competing financial interests or personal relationships that could have appeared to influence the work reported in this paper.

Acknowledgments

This research was partially supported by grants from the National Science Foundation (NSF-EAR-1702319, NSF-EAR-1702293 and NSF-DEB-2048669) to M. Kelly and J. Russell and funding from the Comer Family Foundation to M. Kelly. We thank Rwenzori Mountaineering Services and Rwenzori Trekking Services for logistical support and helpful guidance in performing fieldwork in the Rwenzori Mountains. Fieldwork and sample export were completed under permits from the Uganda Wildlife Authority and the Uganda National Council for Science and Technology. We further thank E. Santos for laboratory assistance.

Appendix A. Supplementary data

Supplementary data to this article can be found online at https://doi.org/10.1016/j.quascirev.2022.107416.

References

- Berke, M.A., Johnson, T.C., Werne, J.P., Grice, K., Schouten, S., Damsté, J.S.S., 2012a. Molecular records of climate variability and vegetation response since the late pleistocene in the lake Victoria basin, East Africa. Quat. Sci. Rev. 55, 59–74.
- Berke, M.A., Johnson, T.C., Werne, J.P., Schouten, S., Damste, J.S.S., 2012b. A mid-Holocene thermal maximum at the end of the African Humid Period. Earth Planet Sci. Lett. 351, 95–104.
- Blaauw, M., Christen, J.A., 2011. Flexible paleoclimate age-depth models using an autoregressive gamma process. Bayesian analysis 6, 457–474.
- Bonnefille, R., Roeland, J., Guiot, J., 1990. Temperature and rainfall estimates for the past 40,000 years in equatorial Africa. Nature 346, 347–349.
- Bony, S., Colman, R., Kattsov, V.M., Allan, R.P., Bretherton, C.S., Dufresne, J.-L., Hall, A., Hallegatte, S., Holland, M.M., Ingram, W., 2006. How well do we understand and evaluate climate change feedback processes? J. Clim. 19, 3445–3482.
- Brook, E.J., Sowers, T., Orchardo, J., 1996. Rapid variations in atmospheric methane concentration during the past 110,000 years. Science 273, 1087–1091.
- Clark, P.U., Dyke, A.S., Shakun, J.D., Carlson, A.E., Clark, J., Wohlfarth, B., Mitrovica, J.X., Hostetler, S.W., McCabe, A.M., 2009. The last glacial maximum. Science 325, 710–714.
- Collins, M., Knutti, R., Arblaster, J., Dufresne, J.-L., Fichefet, T., Friedlingstein, P., Gao, X., Gutowski, W.J., Johns, T., Krinner, G., 2013. Long-term climate change: projections, commitments and irreversibility. In: Climate Change 2013-The Physical Science Basis: Contribution of Working Group I to the Fifth Assessment Report of the Intergovernmental Panel on Climate Change. Cambridge University Press, pp. 1029–1136.
- De Jonge, C., Hopmans, E.C., Zell, C.I., Kim, J.-H., Schouten, S., Damsté, J.S.S., 2014. Occurrence and abundance of 6-methyl branched glycerol dialkyl glycerol tetraethers in soils: implications for palaeoclimate reconstruction. Geochem. Cosmochim. Acta 141, 97–112.
- Doughty, A.M., Kelly, M.A., Russell, J.M., Jackson, M.S., Anderson, B.M., Chipman, J., Nakileza, B., Dee, S.G., 2020. Modeling glacier extents and equilibrium line altitudes in the Rwenzori Mountains, Uganda, over the last 31,000 yr. In: Waitt, R.B., Thackray, G.D., Gillespie, A.R. (Eds.), Untangling the Quaternary Period—A Legacy of Stephen C. Porter. Geological Society of America, 0.
- Eggermont, H., Russell, J.M., Schettler, G., Van Damme, K., Bessems, I., Verschuren, D., 2007. Physical and chemical limnology of alpine lakes and pools in the Rwenzori Mountains (Uganda—DR Congo). Hydrobiologia 592, 151—173.
- Engstrom, D.R., Fritz, S.C., Almendinger, J.E., Juggins, S., 2000. Chemical and biological trends during lake evolution in recently deglaciated terrain. Nature 408, 161–166.
- Favier, V., Wagnon, P., Ribstein, P., 2004. Glaciers of the outer and inner tropics: a different behaviour but a common response to climatic forcing. Geophys. Res. Lett. 31
- Gasse, F., 2000. Hydrological changes in the african tropics since the last glacial

- maximum. Quat. Sci. Rev. 189-211.
- Groos, A.R., Akçar, N., Yesilyurt, S., Miehe, G., Vockenhuber, C., Veit, H., 2021. Nonuniform late pleistocene glacier fluctuations in tropical eastern Africa. Sci. Adv. 7, eabb6826.
- Held, I.M., Soden, B.J., 2006. Robust responses of the hydrological cycle to global warming. J. Clim. 19, 5686–5699.
- Hodell, D.A., Nicholl, J.A., Bontognali, T.R., Danino, S., Dorador, J., Dowdeswell, J.A.,
 Einsle, J., Kuhlmann, H., Martrat, B., Mleneck-Vautravers, M.J., 2017. Anatomy of
 Heinrich Layer 1 and its role in the last deglaciation. Paleoceanography 32,
 284–303
- Hopmans, E.C., Weijers, J.W., Schefuß, E., Herfort, L., Damsté, J.S.S., Schouten, S., 2004. A novel proxy for terrestrial organic matter in sediments based on branched and isoprenoid tetraether lipids. Earth Planet Sci. Lett. 224, 107–116.
- Hopmans, E.C., Schouten, S., Damsté, J.S.S., 2016. The effect of improved chromatography on GDGT-based palaeoproxies. Org. Geochem. 93, 1–6.
- Jackson, M.S., Kelly, M.A., Russell, J.M., Doughty, A.M., Howley, J.A., Chipman, J.W., Cavagnaro, D., Nakileza, B., Zimmerman, S.R., 2019. High-latitude warming initiated the onset of the last deglaciation in the tropics. Sci. Adv. 5, eaaw2610.
- Jackson, M., Kelly, M., Russell, J., Doughty, A., Howley, J., Chipman, J., Cavagnaro, D.,
 Baber, M., Zimmerman, S., Nakileza, B., 2020. Glacial fluctuations in tropical
 Africa during the last glacial termination and implications for tropical climate
 following the Last Glacial Maximum. Quat. Sci. Rev. 243, 106455.
 Kageyama, M., Harrison, S.P., Abe-Ouchi, A., 2005. The depression of tropical
- Kageyama, M., Harrison, S.P., Abe-Ouchi, A., 2005. The depression of tropical snowlines at the last glacial maximum: what can we learn from climate model experiments? Quat. Int. 138, 202–219.
- Kaser, G., Osmaston, H., 2002. Tropical Glaciers. Cambridge University Press.
- Kaufman, D., McKay, N., Routson, C., Erb, M., Dätwyler, C., Sommer, P.S., Heiri, O., Davis, B., 2020. Holocene global mean surface temperature, a multi-method reconstruction approach. Sci. Data 7, 1–13.
- Kelly, M.A., Russell, J.M., Baber, M.B., Howley, J.A., Loomis, S.E., Zimmerman, S., Nakileza, B., Lukaye, J., 2014. Expanded glaciers during a dry and cold last glacial maximum in equatorial East Africa. Geology 42, 519–522.
- Livingstone, D.A., 1962. Age of deglaciation in the ruwenzori range, Uganda. Nature 194. 859–860.
- Livingstone, D.A., 1967. Postglacial vegetation of the ruwenzori mountains in equatorial Africa. Ecol. Monogr. 37, 25–52.
- Loomis, S.E., Russell, J.M., Damsté, J.S.S., 2011. Distributions of branched GDGTs in soils and lake sediments from western Uganda: implications for a lacustrine paleothermometer. Org. Geochem. 42, 739—751.
- Loomis, S.E., Russell, J.M., Ladd, B., Street-Perrott, F.A., Damsté, J.S.S., 2012. Calibration and application of the branched GDGT temperature proxy on East African lake sediments. Earth Planet Sci. Lett. 357, 277—288.
- Loomis, S.E., Russell, J.M., Verschuren, D., Morrill, C., De Cort, G., Sinninghe Damsté, J.S., Olago, D., Eggermont, H., Street-Perrott, F.A., Kelly, M.A., 2017. The tropical lapse rate steepened during the Last Glacial Maximum. Sci. Adv. 3.
- Mackay, A.W., Lee, R., Russell, J.M., 2021. Recent climate-driven ecological changes in tropical montane lakes of Rwenzori Mountains National Park, central Africa. J. Paleolimnol. 65, 219–234.
- Marcott, S.A., Bauska, T.K., Buizert, C., Steig, E.J., Rosen, J.L., Cuffey, K.M., Fudge, T., Severinghaus, J.P., Ahn, J., Kalk, M.L., 2014. Centennial-scale changes in the global carbon cycle during the last deglaciation. Nature 514, 616–619.
- Mark, B., Harrison, S., Spessa, A., New, M., Evans, D., Helmens, K., 2005. Tropical snowline changes at the last glacial maximum: a global assessment. Quat. Int. 138, 168–201.
- Mölg, T., Georges, C., Kaser, G., 2003. The contribution of increased incoming shortwave radiation to the retreat of the Rwenzori Glaciers, East Africa, during the 20th century. Int. J. Climatol.: J. Royal Meteorol. Soc. 23, 291–303.
- Monnin, E., Steig, E.J., Siegenthaler, U., Kawamura, K., Schwander, J., Stauffer, B., Stocker, T.F., Morse, D.L., Barnola, J.-M., Bellier, B., 2004. Evidence for substantial accumulation rate variability in Antarctica during the Holocene, through synchronization of CO2 in the Taylor Dome, Dome C and DML ice cores. Earth Planet Sci. Lett. 224, 45–54.
- Niang, I., Ruppel, O., Abdrabo, M., Essel, A., Lennard, C., Padgham, J., Urquhart, P., 2014. Africa climate change 2014: impacts, adaptation, and vulnerability. Part B: regional aspects. In: Contribution of Working Group II to the Fifth Assessment Report of the Intergovernmental Panel on Climate Change ed VR Barros et al. Cambridge Univ Press, Cambridge, UK.
- Osmaston, H.A., 1965. The Past and Present Climate and Vegetation of Ruwenzori and its Neighbourhood. University of, Oxford.
- Otto-Bliesner, B.L., Russell, J.M., Clark, P.U., Liu, Z., Overpeck, J.T., Konecky, B., Demenocal, P., Nicholson, S.E., He, F., Lu, Z., 2014. Coherent changes of

- southeastern equatorial and northern African rainfall during the last deglaciation. Science 346, 1223–1227.
- Pedro, J., Van Ommen, T., Rasmussen, S., Morgan, V., Chappellaz, J., Moy, A., Masson-Delmotte, V., Delmotte, M., 2011. The last deglaciation: timing the bipolar seesaw. Clim. Past 7, 671–683.
- Pedro, J.B., Bostock, H.C., Bitz, C.M., He, F., Vandergoes, M.J., Steig, E.J., Chase, B.M., Krause, C.E., Rasmussen, S.O., Markle, B.R., 2016. The spatial extent and dynamics of the Antarctic Cold Reversal. Nat. Geosci. 9, 51–55.
- Porter, S.C., 2000. Snowline depression in the tropics during the last glaciation. Ouat. Sci. Rev. 20, 1067–1091.
- Powers, L.A., Johnson, T.C., Werne, J.P., Castaneda, I.S., Hopmans, E.C., Sinninghe Damsté, J.S., Schouten, S., 2005. Large temperature variability in the southern african tropics since the last glacial maximum. Geophys. Res. Lett. 32.
- Reimer, P.J., Austin, W.E., Bard, E., Bayliss, A., Blackwell, P.G., Ramsey, C.B., Butzin, M., Cheng, H., Edwards, R.L., Friedrich, M., 2020. The IntCal20 Northern Hemisphere radiocarbon age calibration curve (0–55 cal kBP). Radiocarbon 62, 725–757.
- Rippert, N., Baumann, K.H., Pätzold, J., 2015. Thermocline fluctuations in the western tropical Indian Ocean during the past 35 ka. J. Quat. Sci. 30, 201–210.
- Romahn, S., Mackensen, A., Groeneveld, J., Pätzold, J., 2014. Deglacial intermediate water reorganization: new evidence from the Indian Ocean. Clim. Past 10, 293–303.
- Russell, J., Eggermont, H., Taylor, R., Verschuren, D., 2009. Paleolimnological records of recent glacier recession in the Rwenzori Mountains, Uganda-DR Congo. I. Paleolimnol. 41. 253–271.
- Russell, J.M., Hopmans, E.C., Loomis, S.E., Liang, J., Damsté, J.S.S., 2018. Distributions of 5-and 6-methyl branched glycerol dialkyl glycerol tetraethers (brGDGTs) in East African lake sediment: effects of temperature, pH, and new lacustrine paleotemperature calibrations. Org. Geochem. 117, 56–69.
- Schilt, A., Baumgartner, M., Schwander, J., Buiron, D., Capron, E., Chappellaz, J., Loulergue, L., Schüpbach, S., Spahni, R., Fischer, H., 2010. Atmospheric nitrous oxide during the last 140,000 years. Earth Planet Sci. Lett. 300, 33–43.
- Seltzer, A.M., Ng, J., Aeschbach, W., Kipfer, R., Kulongoski, J.T., Severinghaus, J.P., Stute, M., 2021. Widespread six degrees celsius cooling on land during the last glacial maximum. Nature 593, 228–232.
- Shakun, J.D., Clark, P.U., He, F., Marcott, S.A., Mix, A.C., Liu, Z., Otto-Bliesner, B., Schmittner, A., Bard, E., 2012. Global warming preceded by increasing carbon dioxide concentrations during the last deglaciation. Nature 484, 49–54.
- Stager, J.C., Ryves, D.B., Chase, B.M., Pausata, F.S., 2011. Catastrophic drought in the Afro-Asian monsoon region during Heinrich event 1. Science 331, 1299–1302.
- Svensson, A., Andersen, K.K., Bigler, M., Clausen, H.B., Dahl-Jensen, D., Davies, S., Johnsen, S.J., Muscheler, R., Parrenin, F., Rasmussen, S.O., 2008. A 60 000 Year Greenland Stratigraphic Ice Core Chronology.
- Taylor, R.G., Mileham, L., Tindimugaya, C., Majugu, A., Muwanga, A., Nakileza, B., 2006. Recent glacial recession in the Rwenzori Mountains of East Africa due to rising air temperature. Geophys. Res. Lett. 33.
- Tierney, J.E., Russell, J.M., Huang, Y., Damsté, J.S.S., Hopmans, E.C., Cohen, A.S., 2008. Northern hemisphere controls on tropical southeast African climate during the past 60,000 years. Science 322, 252—255.
- Tierney, J.E., Zhu, J., King, J., Malevich, S.B., Hakim, G.J., Poulsen, C.J., 2020. Glacial cooling and climate sensitivity revisited. Nature 584, 569–573.
- Tripati, A.K., Sahany, S., Pittman, D., Eagle, R.A., Neelin, J.D., Mitchell, J.L., Beaufort, L., 2014. Modern and glacial tropical snowlines controlled by sea surface temperature and atmospheric mixing. Nat. Geosci. 7, 205–209.
- Vickers, A.C., Shakun, J.D., Goehring, B.M., Gorin, A., Kelly, M.A., Jackson, M.S., Doughty, A., Russell, J., 2021. Similar Holocene glaciation histories in tropical south America and Africa. Geology 49, 140–144.
- Waelbroeck, C., Paul, A., Kucera, M., Rosell-Melé, A., Weinelt, M., Schneider, R., Mix, A.C., Abelmann, A., Armand, L., MARGO, 2009. Constraints on the magnitude and patterns of ocean cooling at the Last Glacial Maximum. Nat. Geosci. 2, 127.
- Webster, P., Streten, N., 1978. Late Quaternary ice age climates of tropical Australasia: interpretations and reconstructions. Quat. Res. 10, 279–309.
- Weijers, J.W., Schouten, S., Spaargaren, O.C., Damsté, J.S.S., 2006. Occurrence and distribution of tetraether membrane lipids in soils: implications for the use of the TEX86 proxy and the BIT index. Org. Geochem. 37, 1680–1693.
- Weijers, J.W., Schouten, S., van den Donker, J.C., Hopmans, E.C., Damsté, J.S.S., 2007. Environmental controls on bacterial tetraether membrane lipid distribution in soils. Geochem. Cosmochim. Acta 71, 703–713.
- Whittow, J., Shepherd, A., Goldthorpe, J., Temple, P., 1963. Observations on the glaciers of the ruwenzori. J. Glaciol. 4, 581–616.